Supporting Information:

Supplementary Information for "Ultrafast Intersystem Crossing and Structural Dynamics of $[Pt(ppy)(\mu-{}^{t}Bu_2pz)]_2$"

Lars Mewes,[*,†,§] Rebecca A. Ingle,[*,†,‖] Sebastian Megow,[‡] Hendrik Böhnke,[‡] Etienne Baranoff,[¶] Friedrich Temps,[‡] and Majed Chergui[†]

†*Laboratoire de spectroscopie ultrarapide and Lausanne Centre for Ultrafast Spectroscopy, Ecole Polytechnique Fédérale de Lausanne, ISIC, FSB Station 6, CH-1015 Lausanne, Switzerland*

‡*Institut für Physikalische Chemie, Christian-Albrechts-Universität zu Kiel, Olshausenstr. 40, D-24098 Kiel, Germany*

¶*School of Chemistry, University of Birmingham, Edgbaston, Birmingham B15 2TT, United Kingdom*

§*Current address: Dynamical Spectroscopies, Department of Chemistry, Technical University of Munich, 85748 Garching, Germany*

‖*Current address: Department of Chemistry, University College London, 20 Gordon Street, WC1H 0AJ, United Kingdom*

E-mail: lars.mewes@tum.de; r.ingle@ucl.ac.uk

Contents

1 Evidence of aggregation in absorption spectroscopy

Since the optical density of a saturated $[Pt(ppy)(\mu\text{-}^{t}Bu_2pz)]_2$ (ppy: 2-phenylpyridine, $^{t}Bu_2pz$: 3,5-di-*tert*-butylpyrazolate), Ptppy, solution in toluene is not sufficient for transient absorption experiments, we choose to increase the concentration via evaporation of the solvent. To ensure that this process does not lead to aggregation of the complexes we perform UV-Vis spectroscopy on the dilute and concentrated solutions. Figure S1 (left panel) shows a good overall agreement between the low (blue) and high (orange) concentration absorption spectra. Slight deviations in the red tail (right panel) of the absorption spectra around 550 - 600 nm are due to the scaling of the low concentration data. The aggregated complexes lead to a decrease of absorption below 400 nm and the appearance of a characteristic broad, low-energy absorption tail between 550 nm and 800 nm (green), due to the formation of low energy aggregate states. For the prepared solutions, aggregation occurs on a time scale of days, i.e. significantly longer than the time needed to perform transient absorption or fluorescence up-conversion experiments.

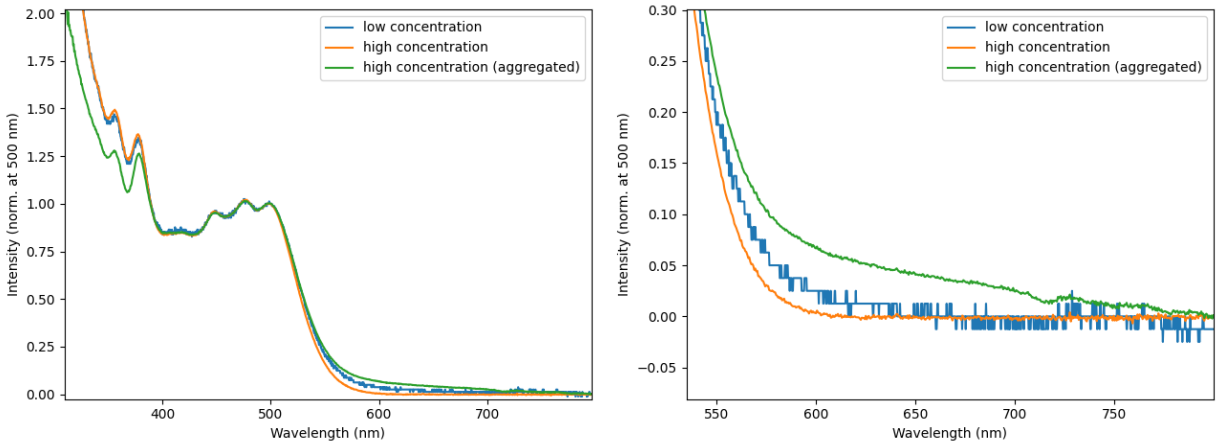

Figure S1: Normalized absorption spectra (at 500 nm) for Ptppy in toluene at a concentration below the limit of solubility (blue) and above the limit of solubility (orange and green). (left) Aggretion is observed as a change in intensity ratio between the spectral features below and above 400 nm, as well as the appearance of a characteristic red tail above 550 nm. The latter can be observed more clearly in the right panel and arises due to formation of low energy aggregate states.

2 Fluorescence decay time constant

The wavelength dependence of the transient fluorescence decay is associated with an activation energy dependent ISC mechanism, as outlined in the main text. Table S1 summarizes the transient fluorescence results, showing the wavelength dependent decay time constant of the subpicosecond component (τ_1).

Table S1: Results of fitting the single wavelength FlUPS data. The instrument-response function (IRF) is described by its standard deviation σ and time zero position t_0. The Gaussian IRF and the exponential functions $n = 1$ and 2 with amplitude A_n and decay constants τ_n describe the impulsive, subpicosecond, and few picosecond signal decay, respectively.

Wavelength [nm]	IRF σ [ps]	IRF t_0 [ps]	A_1	τ_1 [ps]	A_2	τ_2 [ps]
550	0.115	0.27	61.5	0.429		
560	0.117	0.243	126	0.376		
570	0.116	0.242	164	0.522		
580	0.111	0.209	188	0.612		
590	0.103	0.116	223	0.608	10.2	5.31
600	0.13	0.172	236	0.644	10.7	8.49
610	0.13	0.204	212	0.598	21	4.79
620	0.112	0.153	165	0.704	10.9	13.8
630	0.112	0.162	148	0.748	9.5	27.2
640	0.109	0.141	107	0.753	12.7	14.3
650	0.122	0.133	84.6	0.692	8.66	28.9

3 Normalized fluorescence decay curves

To rule out a dynamical Stokes shift and internal vibrational relaxation (IVR), where the vibrational energy relaxes on a given potential energy surface, we normalize and compare the transient fluorescence time traces in Figure S2. The absence of a delayed rise of the longer wavelength components concomitant with the faster decay at shorter wavelengths, allows us to discard the dynamical Stokes shift and IVR. Instead, the increasing time constants (with increasing wavelength) are associated with an energy-dependent intersystem crossing channel.

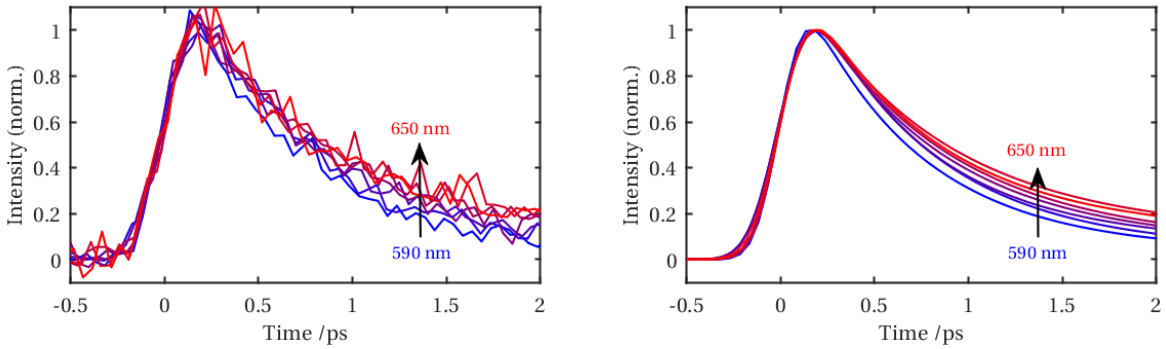

Figure S2: (left) Normalized fluorescence up-conversion data and (right) fits of the data with detection wavelengths varying from 590 nm to 650 nm in 10 nm steps. The increase in the decay time constant for increasing wavelength is not accompanied by an additional rise of the signal. This effect is also observed in the transient absorption data.

4 Correction of steady-state fluorescence

Figure S3 outlines the correction of the steady-state fluorescence spectrum for the spectral responsivity of the fluorometer (Shimadzu RF-5301PC). Briefly, to obtain a reliable, reproducible and comparable fluorescence spectrum, we correct the measured fluorescence spectrum (dashed blue line) by the spectral responsivity (red line) of the instrument, which is obtained using a set of reference standards.[S1] The multiplication of the measured fluorescence spectrum with the spectral responsivity yields the corrected fluorescence spectrum (solid blue line) with a maximum at 710 nm.

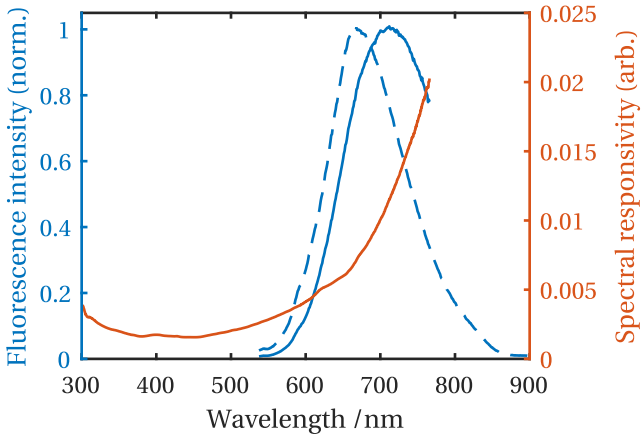

Figure S3: By correcting the measured fluorescence spectrum of Ptppy (dashed blue line) by the spectral responsivity of the instrument (red line) we obtain the true fluorescence spectrum (solid blue line).

5 Global fit of the magic-angle transient absorption

A global fit of the magic-angle transient absorption data reveals a biexponential decay and a constant offset, as described in the main text. Figure S4 shows time traces of a typical fit superimposed onto the raw data. While above 500 nm only two exponential decays (0.7 ps and ∞) are required to fit the data, below 500 nm an intermediate decay with a time constant of $\sim$ 20 ps is necessary. Small deviations can be seen during the signal oscillation before 1 ps and in the intermediate decay below 500 nm, increasing the uncertainty of the $\sim$ 20 ps component. The fit presented here has been caried out in Matlab following the procedure by Fita et al.[S2] Global fits have also been carried out using the Optimus software, developped by Slavov et al.,[S3] leading to similar results.

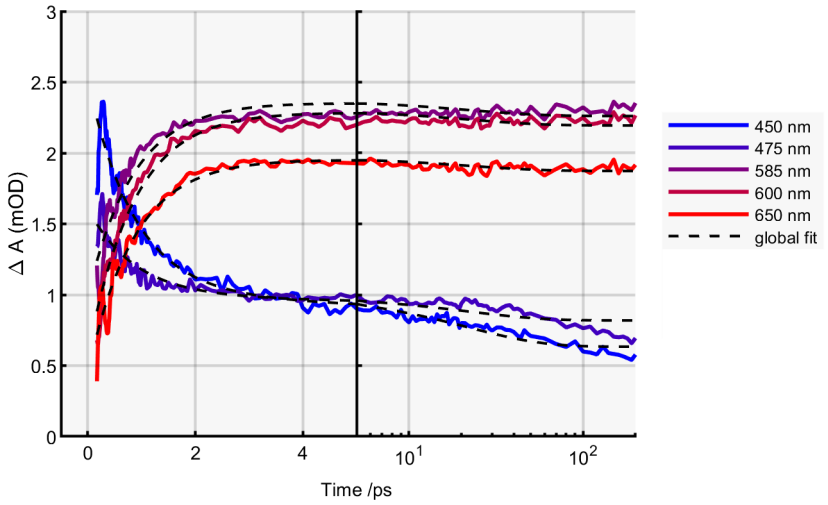

Figure S4: Time traces of the transient absorption signal globally fitted by a sum of two exponential decays and a constant offset.

The residual of a global fit with three exponentials is shown in Figure S5 as a time-wavelength plot (colormap). Superimposed (dashed lines) we show the contour lines of the magic-angle transient absorption data. Note the difference in frequency around 540 nm and 650 nm, associated with the ground- and excited state vibrational coherences (see main text). The slanted shape of the residuals between 540 nm and 610 nm can be explained by the mixing of oscillations with different frequencies in this spectral region.

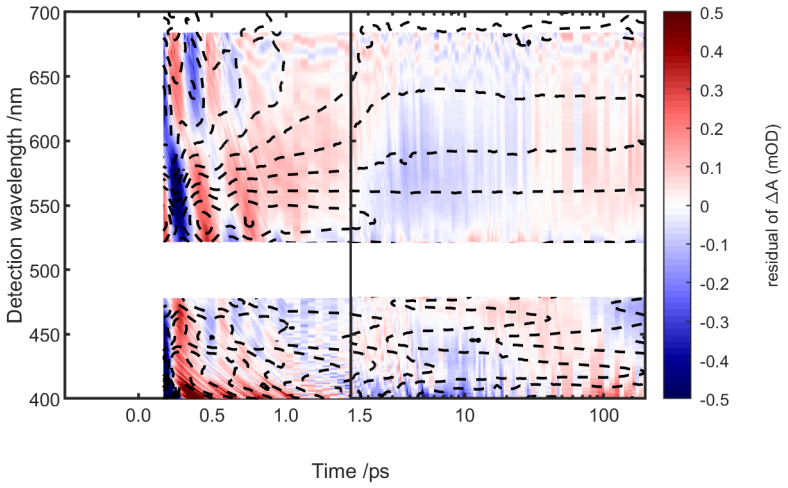

Figure S5: The residuals of a global fit of the signal kinetics reveal the coherences of Ptppy during the first ps, shown as the colormap. The magic-angle transient data is shown for comparison as the overlaying, dashed contour lines.

6 Coherences observed in transient absorption

To estimate the damping time of the coherent oscillation we model the residuals of the magic-angle TA in Figure S6 at 540 nm and 630 nm by a damped cosine function with (a) $\omega = 100\,\mathrm{cm}^{-1}$ and (b) $\omega = 136\,\mathrm{cm}^{-1}$ with an arbitrary phase, multiplied by an exponential damping factor $\exp^{-t/\tau}$. This comparison of the raw data to a model function is preferred to a fitting procedure, since the baseline of the residual deviates from zero. This, in turn, is due to the fact that fitting of an exponential decay to an signal featuring a damped oscillation superimposed on the decay is not trivial. The results show that the coherences decay with $\tau = 0.2$ - 0.5 ps.

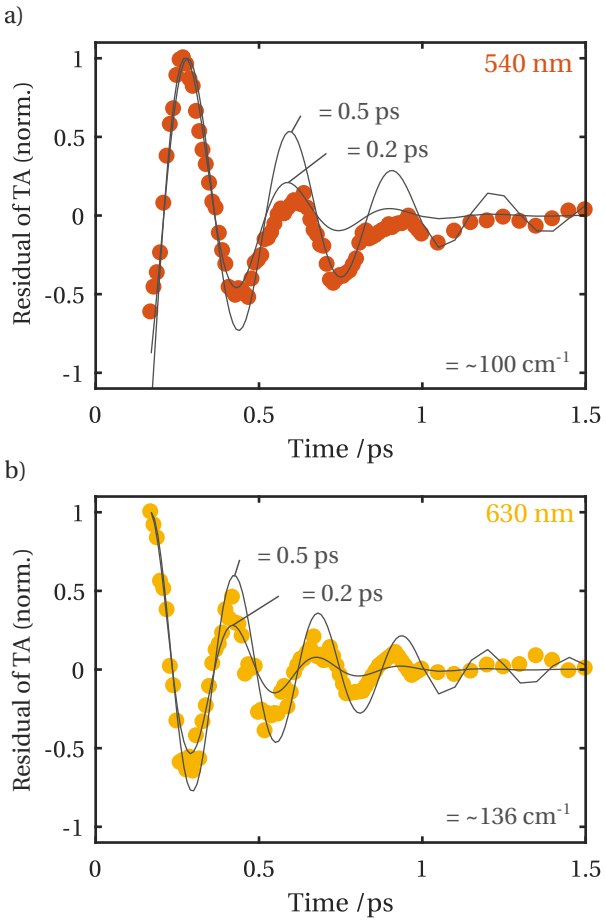

Figure S6: Coherent oscillations observed as the residual of the transient absorption signal at magic-angle at (a) 540 nm and (b) at 630 nm and modelled by a damped cosine function with arbitrary phase and a damping time constant of 0.2 and 0.5 ps.

7 Coherences in transient absorption anisotropy of toluene

In addition to the signal coherences due to Ptppy, we observe the coherent response of the solvent with a period of 155 fs ($\tilde{\nu}$ = 215 cm^{-1}) under parallel and perpendicular relative pump-probe polarization, which we attribute to a rovibrational out-of-plane Raman mode of toluene with a_2'' symmetry, as previously measured with $\tilde{\nu} = 217$ cm^{-1}.[S4,S5] The mechanism that leads to the observation of coherences of a transparent solvent in TA spectroscopy is described in detail by Cho et al. in ref. S6. At magic-angle this coherent signal of the solvent is absent, however, since the anisotropy is calculated from the parallel and perpendicular TA data, the coherence contributes to the oscillations observed in the subpicosecond anisotropy, due to the term $I_{\parallel} - I_{\perp}$, as exemplified in Figure S7.

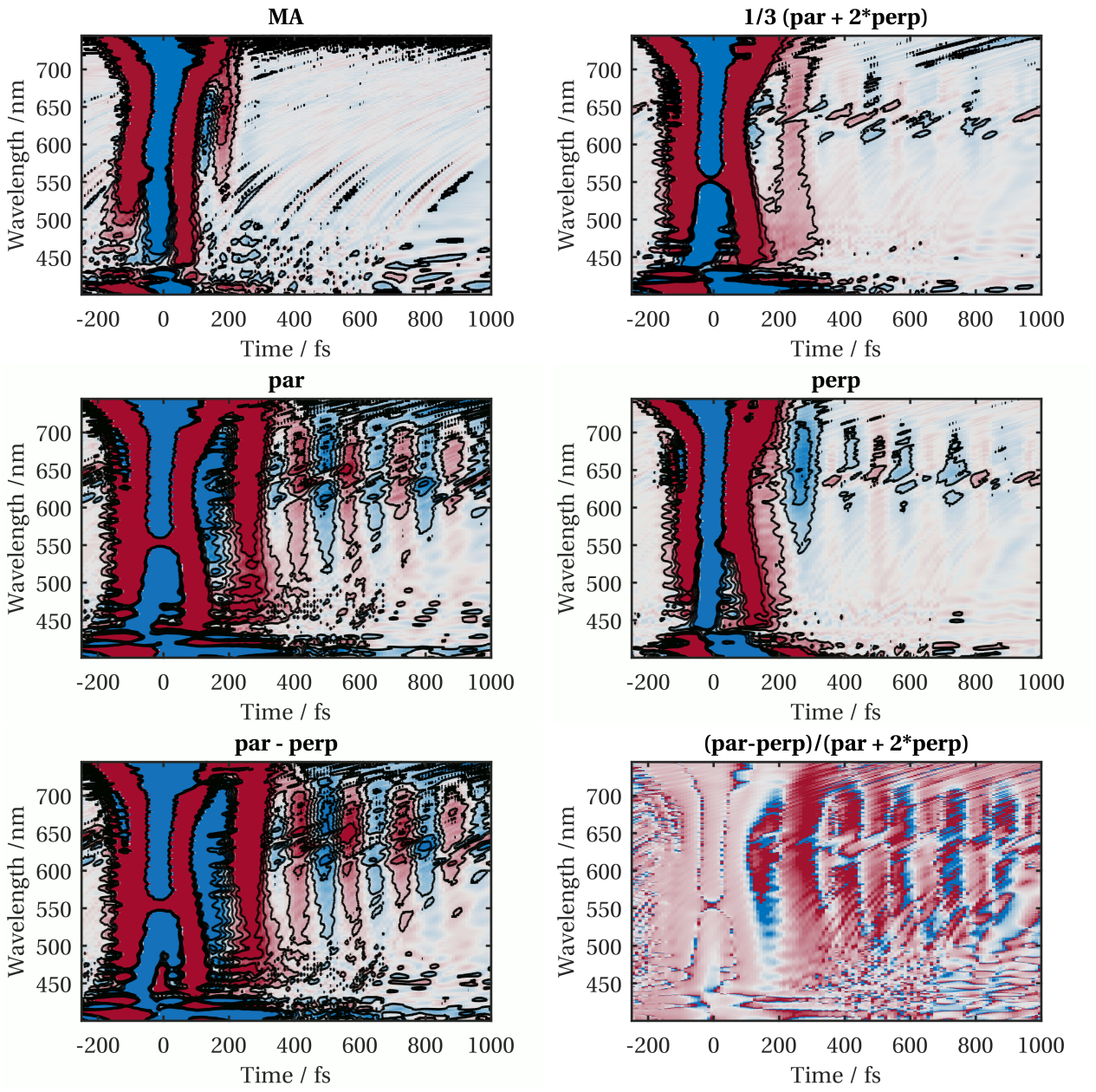

Figure S7: Transient absorption response of toluene with magic-angle (MA), parallel (par) and perpendicular (perp) relative pump-probe polarization, showing a coherent oscillations with 215 cm^{-1} (Raman mode at 217 cm^{-1}).[S5] Calculating the MA signal as 1/3(par+2*perp), shows that the coherences disappear at MA. The difference (par-perp), however, contains the coherence, leading to its appearance in the anisotropy, (par-perp)/(par+2*perp).

8 Calculated photoabsorption cross-section

Vertical excitation energies at the ground state optimised geometries for both the *cis* and *trans* isomers (with and without the effect of an implicit solvent for toluene) are presented as coloured bars in Figure S8. The computed $S_0 \rightarrow S_1$ and $S_0 \rightarrow S_2$ excitation energies are similar for both the *cis* and *trans* isomers and inclusion of the implicit toluene environment has little effect with respect to the gas phase excitation values or oscillator strengths. Notably, the *trans* form exhibits larger oscillator strengths for both the $S_0 \rightarrow S_1$ and $S_0 \rightarrow S_2$ transitions. Figure S8 also shows the calculated wavelength-dependent photoabsorption cross-sections from the nuclear ensemble approach, with and without a toluene environment. The total photoabsorption cross-sections were obtained using the nuclear ensemble average for the first three singlet transitions. The computed spectra show relatively good agreement with the rising edge of the experimental absorption spectrum. For all cases, the major contribution to the total cross-section in this energy window arises from the $S_0 \rightarrow S_1$ transition that spans from 440 nm to 600 nm. By comparison, the computed cross-section corresponding to the $S_0 \rightarrow S_2$ transition is always significantly smaller than the one of $S_0 \rightarrow S_1$ transition. As with the vertical excitation energies, the total photoabsorption cross-sections show only minor differences between the two isomers or with and without the presence of an implicit solvent. At this level of theory, while the inclusion of an implicit solvent for the nuclear ensemble calculation results in a slightly better agreement between the computed photoabsorption cross-section and their experimental counterpart, the differences are minimal. From this, it seems reasonable to conclude that inclusion of a implicit solvent has limited effect on the calculated energies and properties and that gas-phase calculations are a sufficient starting point for comparison to our solution-phase experimental results.

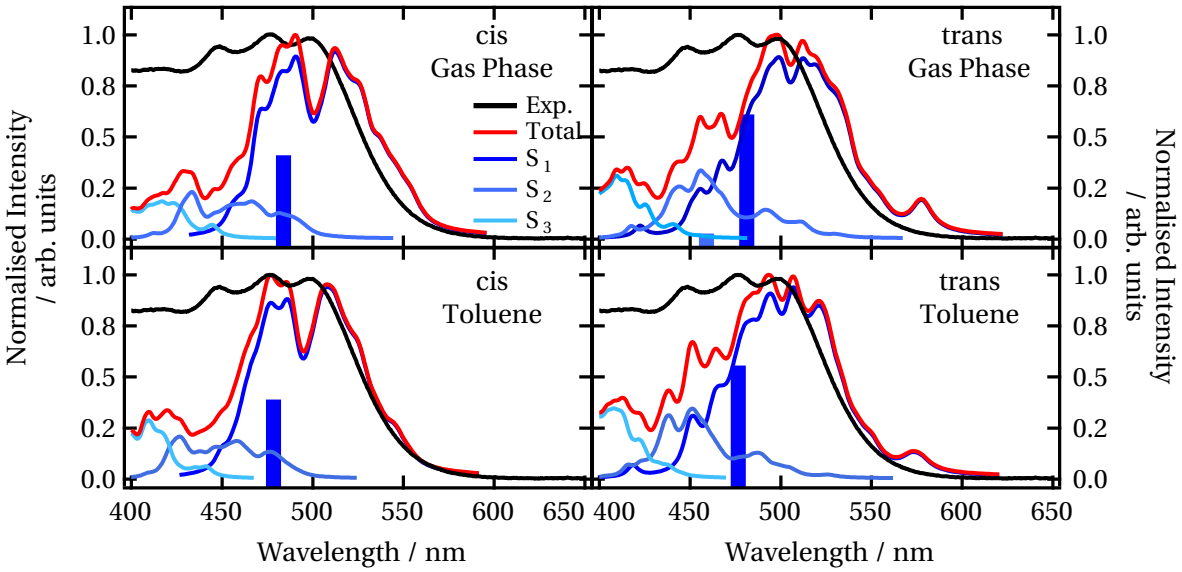

Figure S8: Calculated photoabsorption cross-sections using the nuclear ensemble approach detailed in the text. The upper two plots show the cis (left) and trans (right) isomers calculated in a gas-phase environment (top) and with an implicit solvent mimicking the dielectric response of toluene (bottom). Only the first three singlet excited states are shown here for comparison to the region of interest. The coloured bars are normalised and scaled for the relative oscillator strengths of each transition. The calculated photo absorption cross-sections were normalised to the maximum of the total cross-section and the state contributions were normalised accordingly for comparison to the experimental absorption spectrum. A 0.05 eV Lorentzian line broadening was applied to the sampled excitation energies.

9 Natural transition orbitals

As the ground state to S_1 or T_1 transitions both involve nearly identical donor and acceptor orbitals, the SOC should be weaker as the resulting similarities in the electronic character of the states means the necessary conditions for large non-zero SOC have not been met.[S7] The stronger coupling between the T_2 and S_1 states therefore suggests that the initial, subpicosecond ISC is therefore to the higher-lying T_2 state.

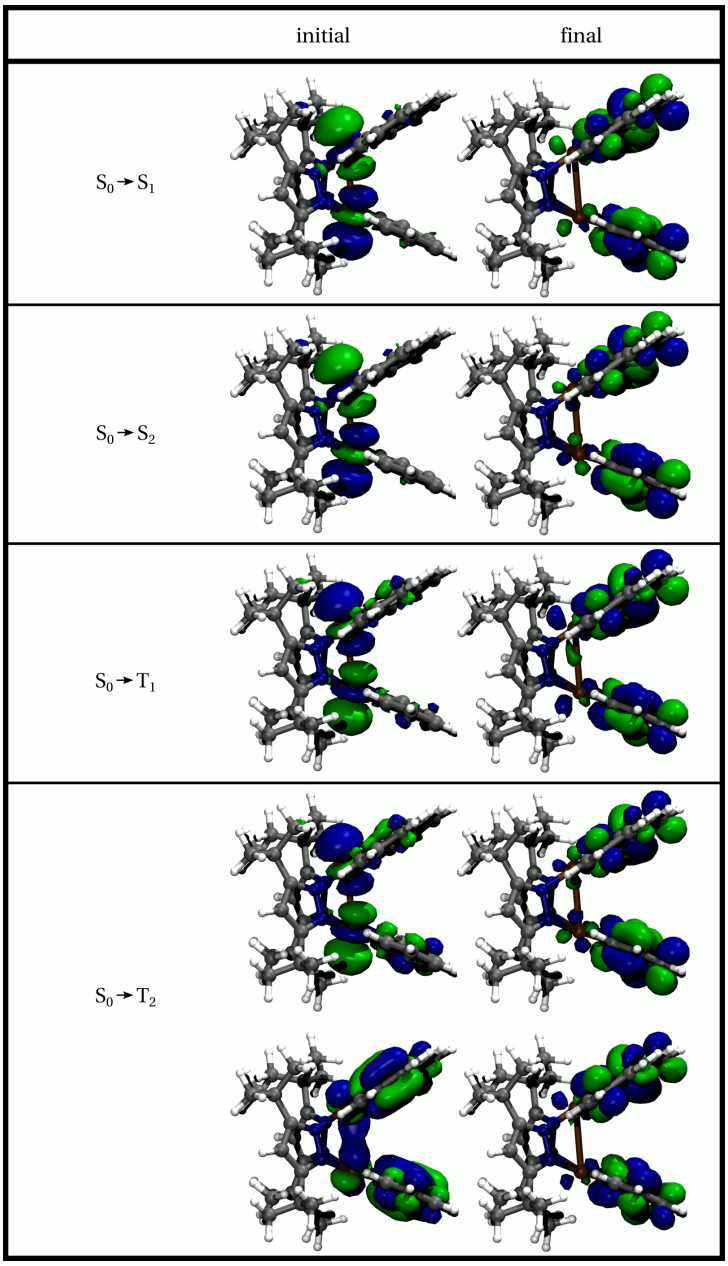

Figure S9: Natural transition orbitals for lowest energy transitions in Ptppy. See main text for details.

References

(S1) Pfeifer, D.; Hoffmann, K.; Hoffmann, A.; Monte, C.; Resch-Genger, U. The Calibration Kit Spectral Fluorescence Standards—A Simple and Certified Tool for the Standardization of the Spectral Characteristics of Fluorescence Instruments. *Journal of Fluorescence* **2006**, *16*, 581–587, DOI: 10.1007/s10895-006-0086-8.

(S2) Fita, P.; Luzina, E.; Dziembowska, T.; Radzewicz, C.; Grabowska, A. Chemistry, Photophysics, and Ultrafast Kinetics of Two Structurally Related Schiff Bases Containing the Naphthalene or Quinoline Ring. *The Journal of Chemical Physics* **2006**, *125*, 184508, DOI: 10.1063/1.2371058.

(S3) Slavov, C.; Hartmann, H.; Wachtveitl, J. Implementation and Evaluation of Data Analysis Strategies for Time-Resolved Optical Spectroscopy. *Analytical Chemistry* **2015**, *87*, 2328–2336, DOI: 10.1021/ac504348h.

(S4) Wilmhurst, J. K.; Bernstein, H. J. The Infrared and Raman Spectra of Toluene, Toluene-α-d_3, m-Xylene, and m-Xylene-$\alpha\alpha'$-d_6[1]. *Canadian Journal of Chemistry* **1957**, *35*, 911.

(S5) Bican, T. H. S.; Schrötter, H. W.; Grošev, V. M. The Raman Spectrum of Toluene Vapour. *Journal of Raman Spectroscopy* **1995**, *26*, 787–790, DOI: 10.1002/jrs.1250260828.

(S6) Cho, M.; Du, M.; Scherer, N. F.; Fleming, G. R.; Mukamel, S. Off-Resonant Transient Birefringence in Liquids. *The Journal of Chemical Physics* **1993**, *99*, 19.

(S7) Yersin, H.; Finkenzeller, W. J. *Highly Efficient OLEDs with Phosphorescent Materials*; Wiley, 2008; DOI: 10.1002/9783527621309.ch1.